Turkish J. Eng. Env. Sci.
30 (2006) , 57 – 68.

Lateral Stiffness of Unreinforced Masonry Circular Columns under Cracked Conditions

M. Arif GÜREL
Harran University, Civil Engineering Department, Şanlıurfa-TURKEY
e-mail: agurel@harran.edu.tr
Murat KISA
Harran University, Mechanical Engineering Department, Şanlıurfa-TURKEY
Feridun ÇILI
İstanbul Technical University, Faculty of Architecture, Taksim, İstanbul-TURKEY

Received 23.06.2005

Abstract

Both walls and columns are main structural elements of monumental buildings. In resisting seismic forces, the lateral stiffness of these elements is an essential parameter. Earthquakes may cause cracks in the masonry, and this reduces the lateral stiffness of the walls and columns. Using an efficient numerical model, this study investigates the effects of cracking on the lateral stiffness of unreinforced masonry cantilever columns with circular cross-section. On the basis of the obtained lateral force versus lateral displacement relationships, the behavior of the columns is characterized by 3 limit states corresponding to the first cracking, maximum resistance and ultimate state. For an example column, the lateral stiffness values at these limit states are determined and compared with each other. The results show that the lateral stiffness is directly related to the displacement level and hence the level of cracking. Implementing a parametric analysis, the effects of the column slenderness, vertical load to column self weight ratio, and the parameter related to the mechanical and physical properties on the lateral stiffness are also investigated.

Key words: Unreinforced masonry, Circular columns, Seismic behavior, Lateral stiffness, Cracking.

Introduction

Besides wood, masonry is the oldest and most important construction material in the history of mankind. It has been used in a wide variety of forms, as a basic material for residential and public buildings and other structures since the earliest days of civilization (Drysdale et al., 1994; Tomaževič, 1999). Even today, masonry is used extensively in many parts of the world for residential and low-rise commercial buildings. Masonry structures will undoubtedly retain their share in the future, especially in developing countries, because of the inherent advantages in material availability, construction simplicity and economic feasibility (Ranjbaran, 1995; Sucuoğlu and Erberik, 1997; Hendry, 2001; Masia et al., 2002; Lu et al., 2005).

A large inventory of the construction heritage is located in areas of high seismicity and they were designed with little or no consideration of seismic loading. Recent earthquakes in various parts of the world have demonstrated that these older masonry structures are extremely susceptible to the forces imposed during such an event. Preservation of this heritage requires a sound understanding of the seismic behavior of masonry structures. It is only through such knowledge that the reliability of existing structures can be analyzed and suitable intervention for their restoration and consolidation can be planned (Bati et al., 1999).

The seismic analysis of masonry building structures having a regular structural plan is generally carried out by equivalent static analysis, assuming that 2 possible directions of the seismic input coin-

cide with those of the principal axes of the structure. If the floors can be assumed to be rigid and firmly connected to the vertical walls and columns, only the walls and columns having significant cross-sectional dimensions in the same direction as the seismic input can be considered to resist the seismic forces, while those directed orthogonally can be neglected because of their negligible lateral stiffness (Çılı, 1978; Bayülke, 1980; La Mendola et al., 1995).

However, in special masonry structures such as monumental buildings (large mosques, cathedrals, etc.), or when the aforementioned assumption cannot be considered realistic, each wall and column has to be examined separately, considering the share of vertical load transmitted to it by the supported deck, arch or dome, its own weight, and the lateral forces (La Mendola et al., 1995). In this case, the determination of the lateral stiffness of the walls and columns realistically becomes an important task.

Seismic actions may cause cracks in the masonry, which has very low resistance to tension. This reduces the uncracked depths of cross-sections. As a result, the lateral stiffness of walls and columns decreases and this causes changes in the vibrational characteristics and so in the dynamic behavior of the structure (Tomaževič, 1999; Clemente et al., 2002). Therefore, the lateral stiffness of walls and columns should be assessed with the consideration of the extent of cracking.

As is well known, the presence or development of cracks does not affect only the behavior and performance of civil engineering structures, but also other engineering structures such as aircraft structures and machine components. Therefore, numerous studies have focused on the effects of cracks on the static and dynamic behavior of engineering structures (Nikpour, 1990; Dimarogonas 1996; Kisa and Brandon, 2000; Kisa, 2004; Gürel and Kısa, 2005).

Cross-sections of columns in monuments show a wide variety of shapes. Rectangular, circular, hexagonal and cruciform sections are the most common. It must be noted that, so far, the analytical and numerical investigations have been devoted to the masonry elements of rectangular cross-section (Yokel, 1971; Frisch-Fay, 1975; La Mendola and Papia, 1993; Romano et al., 1993; De Falco and Lucchesi, 2002). In this study, the lateral stiffness of unreinforced masonry (URM) circular columns is investigated by taking into account the amount of cracking. To this end, the numerical model developed by La Mendola and Papia (1993) for investigating the stability of masonry elements with rectangular cross-section is utilized and extended to circular columns. The model is capable of capturing the cracking and second-order effects efficiently. The column material is assumed to be a homogeneous medium, behaving linear elastically in compression, having an infinite compressive strength and with no tensile strength. The case of a bounded compressive strength and deformability, and a nonlinear stress-strain relationship in compression will be considered in a subsequent work. In the present study, the effects of 3 main parameters, which are related to the column geometry, the loading condition, and the physical and mechanical properties, are also investigated. It must be noted that monolithic and multi-drum masonry columns are outside the scope of the study, because the behavior of these columns under lateral actions is very different from that of the columns investigated in the present work.

Loading Condition and Analysis Model

In this analyis, the URM cantilever (fixed-free ended) column is assumed to be prismatic with a solid circular cross-section as shown in Figure 1(a). In the figure, V indicates a concentrated vertical load transmitted to the column by the supported deck, arch or dome, if any; H is the concentrated lateral load; and $w = W/h$ is the weight per unit height of the column. The column is ideally divided into n finite elements, all having the same height $h_e = h/n$, numbered from 1 to n, starting from the top end, and delimited by $n + 1$ sections, numbered from 0 to n (Figure 1(b)) (La Mendola and Papia, 1993; La Mendola et al., 1995). W/n is the weight of an element, and this force is assumed to be concentrated and applied to the center of gravity of the element.

The deformed shape of the discretized column under the considered loading condition is shown in Figure 2. The deformed shape of the column is assumed to be the combination of successive circle segments. Starting from this assumption, the curvature in an element is taken as constant and this quantity is defined by the value at the upper section for each element. This approximation is justified if the dimensionless height of the elements (the discretization parameter) $\xi = h_e/d = h/nd$ is small enough, i.e. the number n is reasonably high. The system of coordinates $O(x,y)$ is assumed to have its x-axis through the centroid of the top cross-section (Figure 2) (La Mendola et al., 1995).

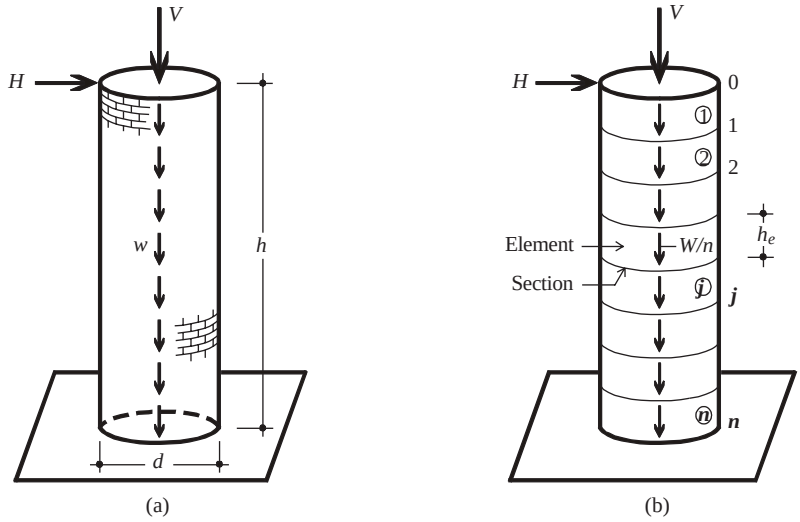

Figure 1. (a) Geometry and loading condition of an unreinforced masonry circular column, (b) discretization of column into elements.

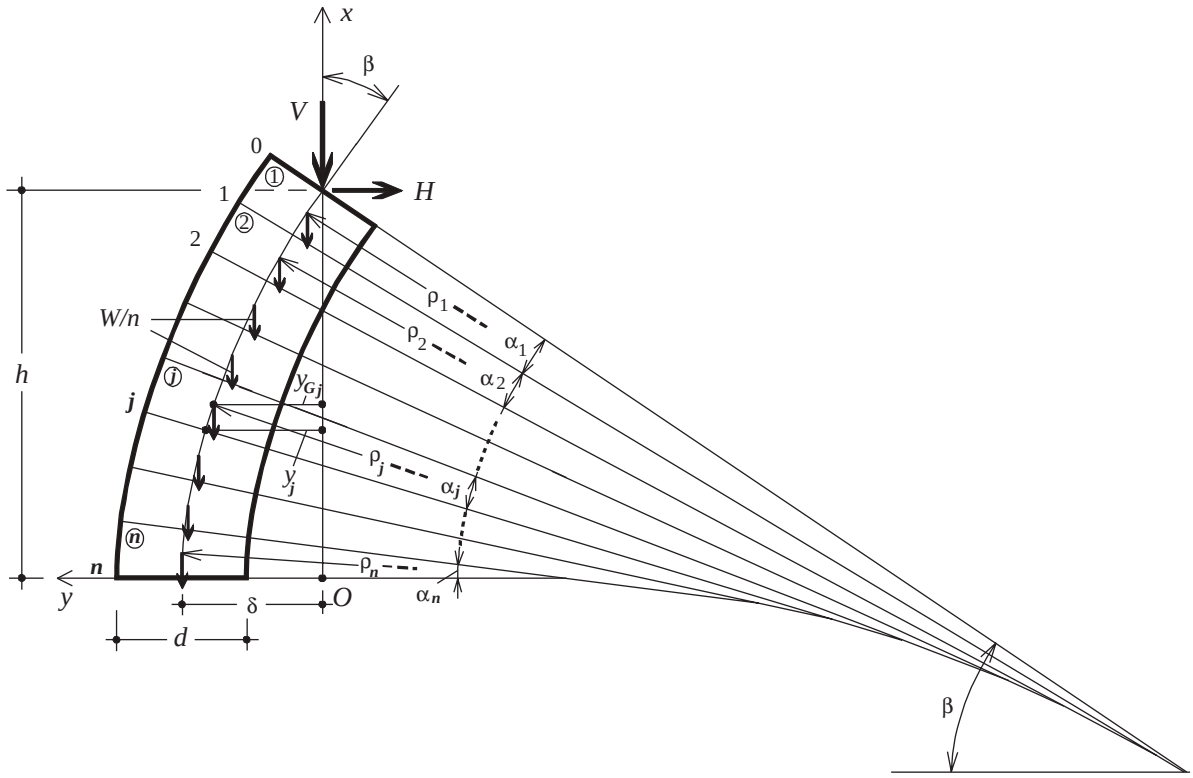

Figure 2. Deformed shape of discretized column.

The numerical model can be used to deduce the whole lateral force − lateral displacement, $H-\delta$, curve and hence lateral stiffness values at uncracked and cracked states of any URM column, by using dimensionless parameters, as explained later.

Using the symbols in Figure 2, the coordinate y of the jth cross-section can be written as

$$y_j = y_{j-1} + \rho_j \left[\cos\left(\beta - \sum_{i=1}^{j} \alpha_i\right) - \cos\left(\beta - \sum_{i=1}^{j-1} \alpha_i\right) \right] \quad (j = 1, 2, ..., n) \tag{1}$$

where β is the rotation of the top cross-section, ρ_j is the radius of curvature of the jth element and $\alpha_j = h_e/\rho_j$ is the angle related to it in the discretized model. Expanding the cosine function in the Taylor's series and retaining the first 3 terms only, Eq. (1) in dimensionless form becomes

$$\frac{y_j}{d} = \frac{y_{j-1}}{d} + \xi\beta + \frac{1}{2}\xi^2\phi_j d - \sum_{i=1}^{j} \xi^2 \phi_i d \quad (j = 1, 2, ..., n) \tag{2}$$

where $\phi_i = 1/\rho_i$ is the curvature of the ith element (La Mendola and Papia, 1993; La Mendola et al., 1995).

Since $y_0 = 0$, and assuming ξ is known, the deformed shape of the column, consistent with the top rotation β, can be obtained using Eq. (2) recursively, starting from the index $j = 1$. This can be done if the curvatures of all the elements over the vertical section in consideration each time are also known.

Eccentricity at the jth cross-section

The resultant axial compressive force and bending moment acting on the jth cross-section can be expressed as

$$N_j = V + j\frac{W}{n} \tag{3a}$$

$$M_j = Vy_j + \frac{W}{n}\sum_{i=1}^{j}(y_j - y_{Gi}) + Hj\frac{h}{n} \tag{3b}$$

where y_{Gi} is the coordinate of the center of mass of the ith element. For the jth element (Figure 2) this quantity can be obtained by the same procedure as used for Eq. (1). In dimensionless form the following expression is obtained

$$\frac{y_{Gj}}{d} = \frac{y_{j-1}}{d} + \frac{1}{2}\xi\beta + \frac{3}{8}\xi^2\phi_j d - \frac{1}{2}\sum_{i=1}^{j}\xi^2\phi_i d \quad (j = 1, 2, ..., n) \tag{4}$$

The ratio between the quantities on the right-hand sides of Eqs. (3b) and (3a) provides the normalized eccentricity in the form

$$\frac{e_j}{d} = \frac{y_j}{d} - \frac{1}{n\frac{V}{W} + j}\sum_{i=1}^{j}\frac{y_{Gi}}{d} + \frac{H}{W}\xi n\frac{j}{n\frac{V}{W} + j} \quad (j = 0, 1, ..., n) \tag{5}$$

For the top cross-section, $j = 0$, this expression gives $e_0/d = y_0/d = 0$ (Figure 2).

Curvature of the jth element

Assuming tensionless material, since little tensile strength is observed in masonry material, with linear stress-strain relationship in compression, the curvature of an element depends on whether its cross-section is uncracked or partially cracked. If the compressive force acting on a section made of tensionless material is within the kern of the section, the section will remain uncracked or else it will be partially cracked. Therefore, 2 different moment-curvature relationships must be considered, depending on the value of the dimensionless eccentricity given by Eq. (5). It is known that the kern of a circular section with radius $r = d/2$ is a circle with the same center and having a radius of $r/4 = d/8$.

When $e_j/d \leq 1/8$, considering the equilibrium condition shown in Figure 3, and using Hooke's Law, the curvature of the $(j + 1)$th element can be expressed as

$$\phi_{j+1} = \frac{\varepsilon_2 - \varepsilon_1}{d} = \frac{\sigma_2 - \sigma_1}{Ed} \tag{6}$$

where E is the modulus of elasticity of masonry in compression and σ_1 and σ_2 are the stresses, which can be written as

$$\sigma_1 = \frac{N_j}{A}\left(1 - \frac{8e_j}{d}\right) \quad , \quad \sigma_2 = \frac{N_j}{A}\left(1 + \frac{8e_j}{d}\right) \tag{7a,b}$$

where $A = \pi d^2/4$ is the area of the cross-section. Substituting these expressions of σ_1 and σ_2 into Eq. (6), the dimensionless curvature of the $(j + 1)$th element becomes

$$\phi_{j+1}d = \frac{N_j}{EA}\frac{16e_j}{d} \tag{8}$$

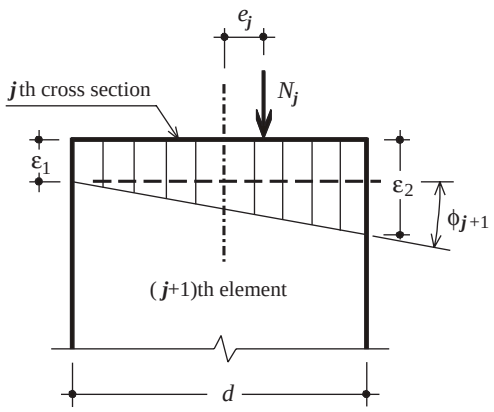

Figure 3. Strains and curvature at an uncracked cross-section.

If the dimensionless eccentricity is greater than $1/8$, $e_j/d > 1/8$, the cross-section is partially cracked (Figure 4). In this case, the curvature cannot be obtained easily, because the location of the neutral axis, s, is not determined. A trial-and-error procedure is needed to find the position of the neutral axis, and then find $\sigma_{\max} = \sigma_0$, $\varepsilon_{\max} = \varepsilon_0$ and curvature. Here, for the neutral axis depth and the maximum stress in section, expressions given in the textbook of Strength of Materials (İnan, 1988) are used. In this reference, the following expressions are given for the neutral axis depth and the maximum compressive stress, respectively:

$$s \cong \frac{1}{2}\left[2.33\left(1-2\frac{e_j}{d}\right)+0.58\left(1-2\frac{e_j}{d}\right)^3\right]d \quad (9a)$$

$$\sigma_0 \cong \frac{4\left[0.372+0.056\left(1-2\frac{e_j}{d}\right)\right]N_j}{d^2\left(1-2\frac{e_j}{d}\right)^{\frac{3}{2}}} \quad (9b)$$

Numerical calculations carried out by the authors have shown that the values obtained for the neutral axes depths and the maximum stresses using Eqs. (9a) and (9b) are almost equal to those calculated with the trial-and-error procedure.

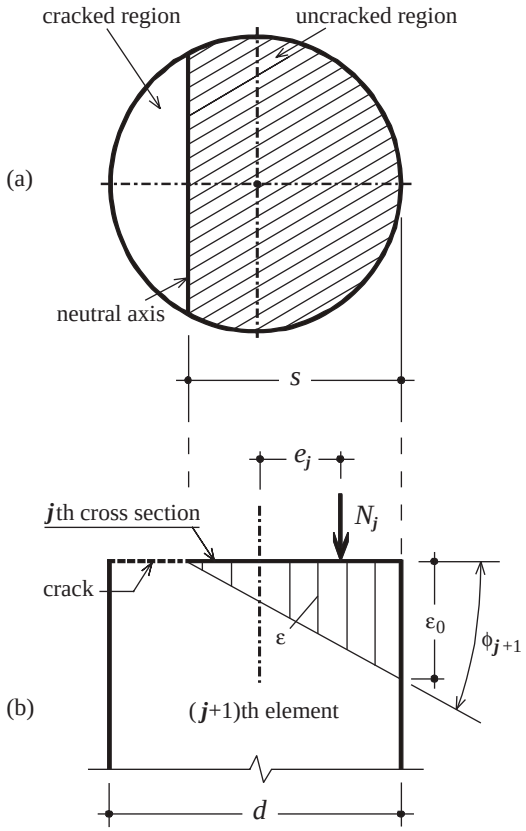

Figure 4. (a) A partially cracked cross-section, (b) strains and curvature at the section.

The curvature in the partially cracked cross-section case can be written as (Figure 4)

$$\phi_{j+1} = \frac{\varepsilon_0}{s} = \frac{\sigma_0}{Es} \quad (10)$$

Substituting Eqs. (9a) and (9b) into Eq. (10), the curvature of the $(j+1)$th element in dimensionless form becomes

$$\phi_{j+1}d = \frac{N_j}{EA}\times \frac{2\pi\left[0.372+0.056\left(1-2\frac{e_j}{d}\right)\right]}{\left[2.33\left(1-2\frac{e_j}{d}\right)+0.58\left(1-2\frac{e_j}{d}\right)^3\right]\left(1-2\frac{e_j}{d}\right)^{\frac{3}{2}}} \quad (11)$$

Equations (8) and (11) can be given under a single expression as

$$\phi_{j+1}d = \frac{N_j\lambda_j}{EA} \quad (12)$$

in which

$$\lambda_j = \begin{cases} 16e_j/d & \text{for} \quad 0 \le \dfrac{e_j}{d} \le \dfrac{1}{8} \\ \dfrac{2\pi[0.372 + 0.056\,(1 - 2e_j/d)]}{\left[2.33\,(1 - 2e_j/d) + 0.58\,(1 - 2e_j/d)^3\right]\,(1 - 2e_j/d)^{3/2}} & \text{for} \quad \dfrac{1}{8} \le \dfrac{e_j}{d} < \dfrac{1}{2} \end{cases} \tag{13}$$

When Eq. (3a) is introduced into Eq. (12) and with certain operations, the dimensionless curvature of the $(j + 1)$th element takes the following form

$$\phi_{j+1}d = \frac{\gamma d}{E}\xi\left(n\frac{V}{W} + j\right)\lambda_j \qquad (j = 0, 1, 2, ..., n-1) \tag{14}$$

where $\gamma = W/(\pi d^2 h/4)$ is the weight of the unit volume of the column.

Solution Procedure

For an URM circular column fixed at the base and free at the top, the whole $H - \delta$ curve, corresponding to the assigned values of the vertical load to column self weight ratio V/W and the parameter $\gamma d/E$, can be deduced using Eqs. (5), (13), (14), (2) and (4) in sequence. For this purpose, the column is ideally divided into a sufficiently high number of elements, and hence the discretization parameter ξ becomes known. It must be noted that the accuracy of the results does not change if the number of elements is increased above a certain value, but it is advisable to choose an n value not less than 20. Starting with a small initial value of the lateral force H and assigning a trial value of the top rotation β, using Eq. (5) and then Eqs. (13) and (14) for $j = 0$, one obtains $\phi_1 d = 0$; therefore, Eq. (2) provides the $y_1/d = \xi\beta$. Then, using the equations just mentioned in the same order but for $j = 1$, one obtains y_2/d, and so on.

When the procedure stops, i.e. when the index j reaches the value $n - 1$ in Eq. (14), the following convergence criterion is controlled, which implies zero rotation at the base of the cantilever column:

$$\beta = \sum_{i=1}^{n}\alpha_i = \sum_{i=1}^{n}\xi\phi_i d \tag{15}$$

It will be repeated with a decreased value of β, if $\beta - \sum_{i=1}^{n}\xi\phi_i d > 0$, and an increased value of β will be used in the opposite case. When convergence on β is reached, in other words, after the actual value of this rotation corresponding to the assigned value of H is iteratively determined, the deflection $y_n = \delta$ can be calculated directly from Eq. (2).

Repeating the procedure with variation in β and adopting small increases for this quantity, the whole curve H versus δ can be plotted and hence critical (H , δ) pairs that represent characteristic points (limit states) can be determined. The maximum value of β consistent with the equilibrium of the column corresponds to the limit condition at which the dimensionless eccentricity at the base cross-section is equal to 0.5 (La Mendola et al., 1995). Because of the tensionless material assumption, it is evident that the equilibrium cannot be satisfied for the greater values of the dimensionless eccentricity.

Application and Discussion

In this section, firstly, the preceding procedure is used to deduce the whole lateral force versus lateral displacement, $H - \delta$, curve for an URM circular column. For this cantilever column (Figure 5) the following data are considered: $h = 7.5$ m; $d = 1.0$ m; $\gamma = 18$ kN/m^3; $E = 3600$ MPa; $V = 106$ kN; and $W = \gamma(\pi d^2 h/4) \cong 106$ kN. Consequently, the column has $h/d = 7.5$; $\gamma d/E = 0.5\times10^{-5}$; and $V/W = 1.0$. The column is ideally divided into 30 finite elements, so that the discretization parameter ξ is 0.25.

The result of the procedure is shown in Figure 6. The curve in this figure highlights the key features of the behavior of the column. As can be seen, initially, the column deforms in a linear manner; however, it cracks when the lateral force reaches approximately 4.77 kN value, H_{cr}. The column continues to carry increasing force beyond initial cracking, but loses lateral stiffness as the first crack grows and new cracks are formed. When the lateral force attains its maximum value $H_{\max} \cong 10.78$ kN, producing the deflection $\delta \cong 67.01$ mm, the maximum dimensionless eccentricity at the base of the column is $e/d = 0.429$. Beyond this point, up to the limit value of $e/d = 0.5$,

the state of the column is unstable.

Figure 7 shows the highly magnified normalized deformed shape of the column at the maximum resistance stage. The high curvature caused by extensive cracking in the base region compared with the upper part of the column can be easily discerned.

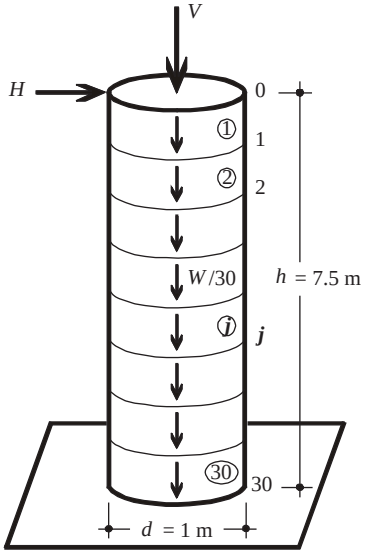

Figure 5. Masonry column considered.

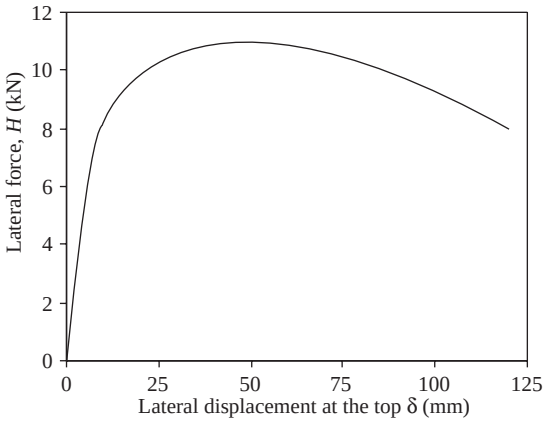

Figure 6. Numerically obtained lateral resistance – lateral displacement curve.

To see the effect of cracking on the lateral stiffness of the column, the resistance curve obtained numerically is idealized with a trilinear relationship, shown in Figure 8. Three characteristic points (limit states) are defined on the resistance curve, determined by 3 pairs of parameters (Table 1):

(a) *Elastic* (*crack*) *limit*: determined by lateral force H_{cr} and displacement δ_{cr} at the formation of the first significant crack in the column, which changes the initial stiffness,

(b) *Maximum resistance*: determined by lateral force $H_{\max}$ and displacement $\delta_{H\max}$ at the attained maximum resistance of the column, and

(c) *Ultimate state*: determined by the lateral resistance $H_{\delta\max}$ at maximum attained displacement $\delta_{\max}$ just before the collapse (Tomaževič and Klemenc, 1997; Tomaževič, 1999).

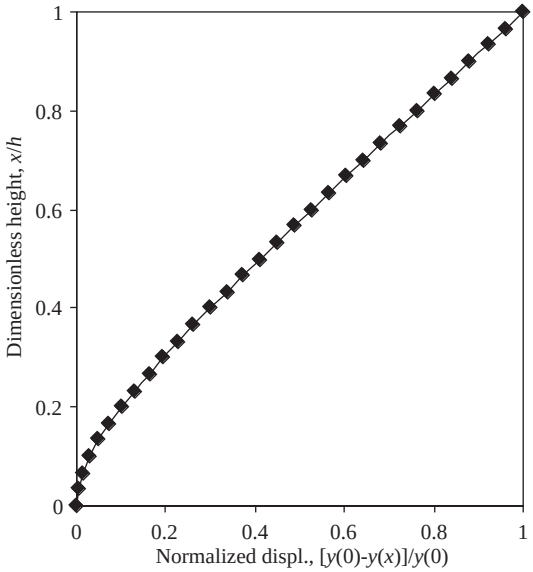

Figure 7. Normalized deformed shape of the column at the attained maximum resistance.

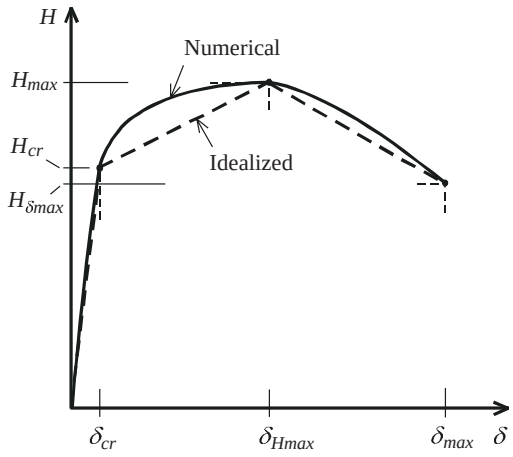

Figure 8. Idealization of numerically obtained curve.

Table 1. Parameters of numerically obtained resistance curve.

H_{cr} (kN)	δ_{cr} (mm)	$H_{\max}$ (kN)	$\delta_{H\max}$ (mm)	$H_{\delta\max}$ (kN)	$\delta_{\max}$ (mm)
4.77	4.18	10.78	67.01	8.09	120.61

Masonry is an inelastic structural material that does not behave elastically even in the range of small deformations. However, for practical reasons, the elastic lateral stiffness of the column, K_e, defining the slope of the first branch of the idealized resistance curve, is determined as the ratio between the lateral load and displacement at the formation of the first significant crack in the column (Tomaževič and Klemenc, 1997):

$$K_e = K_{cr} = H_{cr}/\delta_{cr} \tag{16}$$

For the example column, 4.77 kN and 4.18 mm values are obtained for H_{cr} and δ_{cr} , respectively; thus, one obtains $K_e = 4.77 \ / \ 4.18 = 1.141$ kN/mm value, according to Eq. (16).

From the strength of materials, the lateral stiffness of a slender cantilever column made of linear-elastic material and having a constant cross-section is

$$K_e = 3EI/h^3 \tag{17}$$

where E, I and h are the modulus of elasticity of the column material, moment of inertia of the column cross-section, and height of the column, respectively. Equation (17) does not take into account the self weight of the column or any vertical top load. When the lateral stiffness of the considered column is calculated using this equation, $K_e = 1.256$ kN/mm is obtained. Thus, the ratio between the numerical result and the value obtained with Eq. (17) becomes $1.141/1.256 = 0.91$.

After cracking, the lateral stiffness of the column is defined as the secant stiffness, $K = H/\delta$, i.e. as the ratio between the lateral resistance of the column and the corresponding displacement. The values of secant stiffness, calculated at the characteristic points of the lateral force versus lateral displacement curve, are given in Table 2. In order to determine the degree of secant stiffness degradation, the calculated values are also expressed in terms of the elastic stiffness, K_e, of the column.

Table 2. Stiffness values and stiffness degradation at characteristic points of lateral resistance curve.

K_e (kN/mm)	$K_{H\max}$ (kN/mm)	$K_{H\max}/K_e$	$K_{\delta\max}$ (kN/mm)	$K_{\delta\max}/K_e$
1.141	0.161	0.14	0.067	0.06

Variation of the lateral stiffness of the column as a function of lateral displacements is shown in Figure 9. It can be seen that the $K-\delta$ curve has an ascending initial branch. The increase in the lateral stiffness in this part can be interpreted as follows. As explained earlier, the solution procedure begins with a small value of the lateral force. This force pushes the column and produces small displacements, but the column does not exert its full lateral resistance against this small force. The column shows a similar behavior up to the application of H_{cr}, which causes the first crack in the column, and the column displays its maximum lateral stiffness at this moment. As expected, after the maximum a sharp decrease in the lateral stiffness with increasing displacements is observed (Figure 9).

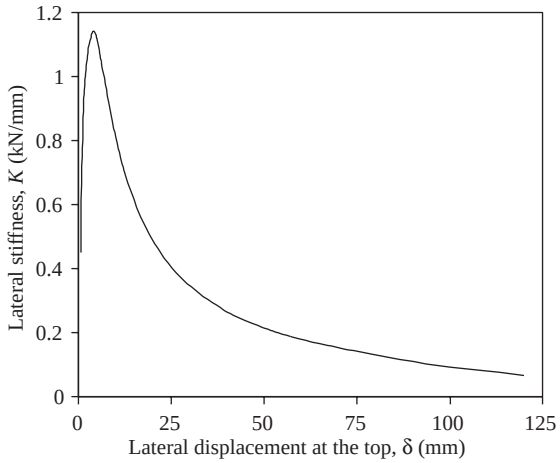

Figure 9. Stiffness variation of the considered column depending on the lateral displacements.

In the second part of this section, the effects of some parameters on the lateral stiffness of URM circular columns are investigated. The parameters examined refer to the geometry, loading, and physical and mechanical properties. For the geometry, we considered column slenderness, h/d. The loading parameter investigated was the vertical load to column self weight ratio, V/W. The physical and mechanical property considered was the parameter $\gamma d/E$, which La Mendola et al. (1995) called the *flexibility parameter*. Here γ is the weight per unit volume of the column.

Effect of column slenderness, h/d

Figure 10 illustrates lateral resistance – lateral displacement curves obtained for 3 columns having different slenderness values of $h/d = 5$, 7.5 and 10, but

constant $V/W = 1$ and $\gamma d/E = 0.5 \times 10^{-5}$. It is obvious from the figure that the initial slope, i.e. elastic lateral stiffness and maximum resistance, increases with decreasing slenderness. Variations of lateral stiffness depending on the lateral displacement are shown in Figure 11. The evident difference between the lateral stiffness values in the small displacement range can be seen from the figure. Lateral stiffness values at characteristic points are given in Table 3.

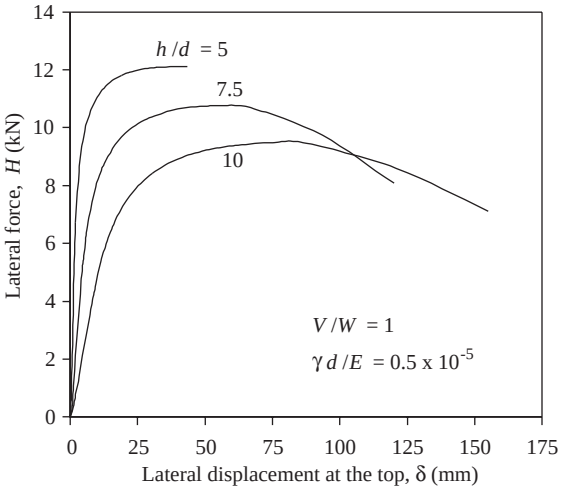

Figure 10. Lateral resistance – lateral displacement curves at various slenderness h/d for constant V/W and $\gamma d/E$.

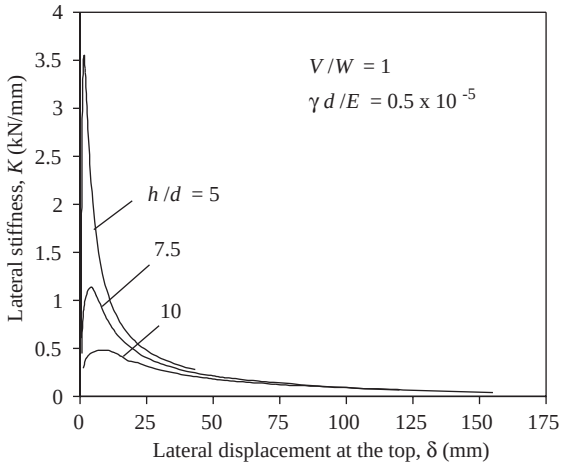

Figure 11. Variations of lateral stiffness with respect to lateral displacement for various values of slenderness h/d.

Effect of vertical load to column self weight ratio, V/W

Figure 12 shows the lateral resistance – lateral displacement curves of a column having $h/d = 7.5$ and $\gamma d/E = 0.5 \times 10^{-5}$ for different vertical load to column self weight ratios of $V/W = 0$, 1, 2.5, 5 and 7.5. It can be seen that the curves obtained for different V/W values have almost the same initial slope. For greater values of the V/W ratio, higher maximum resistance values are obtained. Moreover, maximum displacements are also increased. Variations of lateral stiffness with respect to the lateral displacement are shown in Figure 13. It is seen that there is a negligible positive effect of the V/W ratio on the lateral stiffness in the very small displacement range, while it has an important influence in the moderate and large displacement regions. Lateral stiffness values at characteristic points are given in Table 4.

Table 3. Lateral stiffness values at characteristic points for various values of slenderness h/d.

K (kN/mm)	Slenderness, h/d		
	5	7.5	10
K_e	3.555	1.141	0.486
$K_{H\,\max}$	0.280	0.161	0.110
$K_{\delta\,\max}$	0.280	0.067	0.046

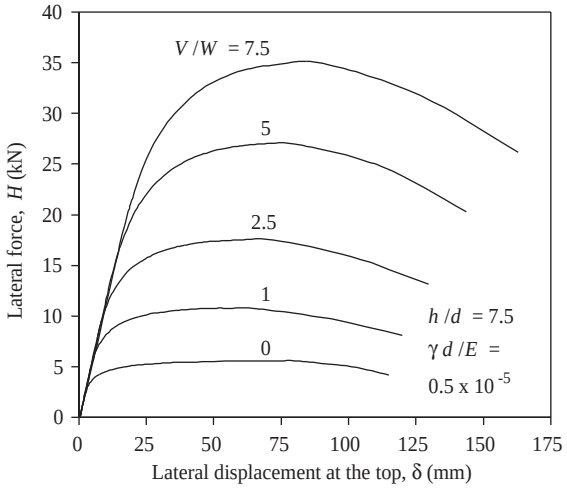

Figure 12. Lateral resistance – lateral displacement curves at various vertical load to column self weight ratios V/W for constant h/d and $\gamma d/E$.

Effect of the flexibility parameter, $\gamma d/E$

Figure 14 shows the lateral resistance – lateral displacement curves of a column having $h/d = 7.5$ and $V/W = 1$ for different values of the parameter of $\gamma d/E = 0.25 \times 10^{-5}$, 0.5×10^{-5} and 1.0×10^{-5}.

It can be seen that there are obvious differences between the initial slopes of the curves corresponding to different values of $\gamma d/E$. When $\gamma d/E$ decreases, both elastic stiffness and maximum resistance increase; however, maximum lateral displacement decreases. Variations of lateral stiffness with respect to lateral displacement are shown in Figure 15. It is clearly seen that $\gamma d/E$ is efficient in the small displacement range. Lateral stiffness values at characteristic points are given in Table 5.

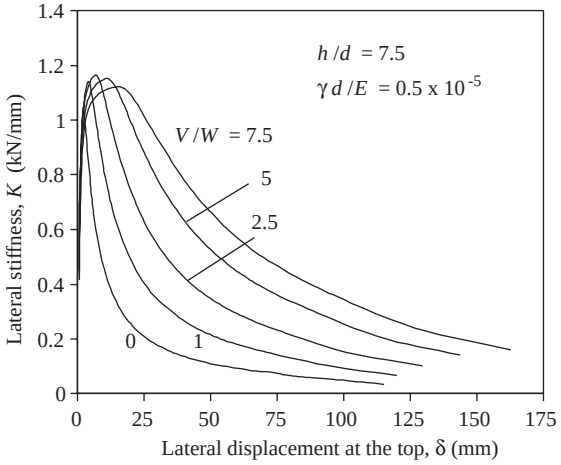

Figure 13. Variations of lateral stiffness with respect to lateral displacement for various values of vertical load to column self weight ratios V/W.

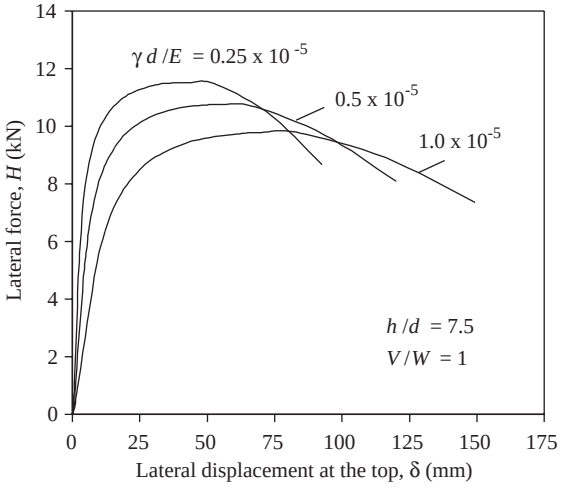

Figure 14. Lateral resistance – lateral displacement curves at various $\gamma d/E$ values for constant h/d and V/W.

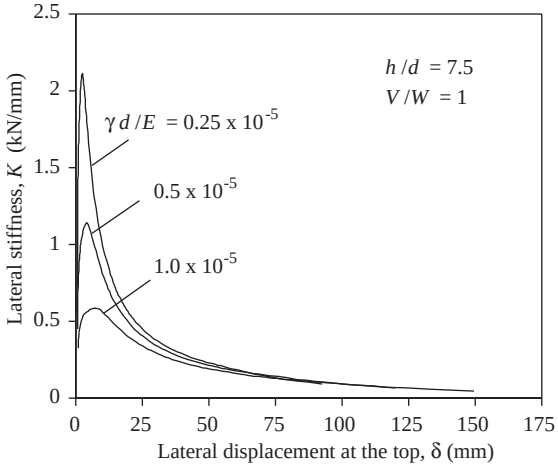

Figure 15. Variations of lateral stiffness with respect to lateral displacement for various values of $\gamma d/E$.

Table 4. Lateral stiffness values at characteristic points for various values of V/W ratio.

K (kN/mm)	Vertical load to column self weight ratio, V/W				
	0	1	2.5	5	7.5
K_e	1.044	1.141	1.165	1.153	1.123
$K_{H\max}$	0.066	0.161	0.243	0.339	0.386
$K_{\delta\max}$	0.035	0.067	0.101	0.141	0.161

Table 5. Lateral stiffness values at characteristic points for various values of $\gamma d/E$.

K (kN/mm)	$\gamma d/E$ parameter		
	0.25×10^{-5}	0.5×10^{-5}	1.0×10^{-5}
K_e	2.111	1.141	0.588
$K_{H\max}$	0.225	0.161	0.118
$K_{\delta\max}$	0.094	0.067	0.049

Effects of imperfections

Monumental buildings are subject to aging effects and many different imperfections may have been formed in these structures over the course of time. Deflection or bulging of walls and columns under the effects of carried loads and/or material creep, tilting of walls and columns due to differential settlement of foundations, and edge damage at the base of walls and columns, depicted in Figure 16, are only some of them. It is obvious that such imperfections affect the lateral stiffness of walls and columns negatively.

For example, edge damage in a column base (Figure 16(c)) causes an effective increase in the slenderness of the column, and therefore decreases its lateral stiffness. The effects of several imperfections are additive and the lateral stiffness and earthquake performance of the main structural elements of monumental and historical buildings may be substantially reduced by the cumulative effect of these imperfections (Psycharis et al., 2000; Gürel and Çılı, 2001).

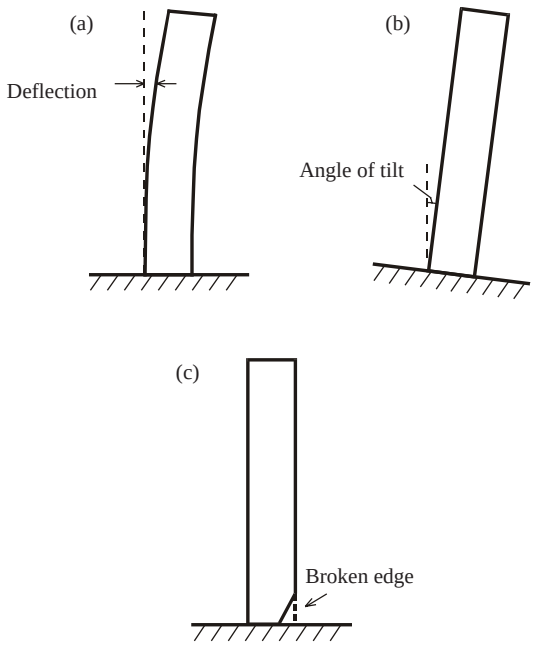

Figure 16. Some structural imperfections: (a) initial deflection, (b) initial tilt, (c) edge damage at the column base.

Summary and Conclusions

The paper presents the lateral stiffness analysis of URM cantilever columns with circular cross-section. The columns are modeled as prismatic cantilevers undergoing their own weights, concentric vertical top loads and static lateral top loads having increasing magnitude. The material behavior is assumed to be linear in compression, but since the masonry cracks when the lateral loading on the columns is increased, the problem is nonlinear. The solution is achieved using a numerical model capable of capturing the cracking and second-order effects efficiently. The main conclusions obtained from the study can be summarized as follows:

1) The numerical model employed is very suitable for obtaining the whole lateral force – lateral displacement, $H - \delta$, relationships of URM circular columns, since it takes into account the cracking and the second-order effects efficiently. Utilizing $H - \delta$ knowledge, the lateral stiffness of a column at any displacement level can be calculated. Using the same numerical model, columns having cross-sectional shapes other than circular can be analyzed similarly.

2) The lateral stiffness of an URM circular column depends not only on the slenderness, material properties and vertical load ratio, but also on the displacement level and hence the extent of cracking.

3) The monotonic lateral load – lateral displacement behavior of URM slender circular columns can be characterized by 3 limit states corresponding to the elastic limit, maximum resistance and ultimate state. Elastic lateral stiffness values of the columns decrease dramatically with increasing lateral displacements caused by cracking and second-order effects.

4) Both the elastic and cracked lateral stiffness of a column decrease with increasing column slenderness ratio, h/d, and the flexibility parameter, $\gamma d/E$, especially in the small and moderate displacement ranges (Figures 11 and 15, Tables 3 and 5). Elastic lateral stiffness increases with the increase in vertical load to column self weight ratio, V/W, up to a certain value, but then decreases with increasing V/W values. However, cracked stiffness values increase with increasing V/W ratios (Figure 13, Table 4).

5) Although they have not been considered in the present study, imperfections such as tilting or reduced contact area at the column base can be taken into account and their effects on the lateral stiffness can be investigated quantitively. Without performing an analysis it can be said that any imperfection decreases the lateral stiffness. It is evident that the lateral stiffness decreases as the magnitude of imperfection increases.

6) The analysis of the present study is mainly for slender circular columns. However, extension to squat columns can be carried out by considering the contribution of shear deformations. Other possible extensions of the present analysis are the inclusion of material nonlinearity as well as the variation of the cross-section of the column (nonprismatic columns), which are left for future studies.

References

Bati, S.B., Ranocchiai, G. and Rovero, L., "Suitability of Micromechanical Model for Elastic Analysis of Masonry", Journal of Engineering Mechanics, ASCE, 125, 922-929, 1999.

Bayülke, N., Masonry Structures, Turkish Republic, Ministry of Settlement and Reconstruction. Ankara, 1980, (in Turkish).

Clemente, P., Bongiovanni, G. and Buffarini G., "Experimental Seismic Behavior of a Cracked Masonry Structure", Proceedings of the 12th European Conference on Earthquake Engineering, London, Paper No:104, 2002.

Çılı, F., "Analysis of Masonry Structures for Lateral Loads", Bulletin of Earthquake Research Institute, Turkish Republic, Ministry of Settlement and Reconstruction, 22, 7-25, 1978, (in Turkish).

De Falco, A. and Lucchesi M., "Stability of Columns with No Tension Strength and Bounded Compressive Strength and Deformability", International Journal of Solids and Structures, 39, 6191-6210, 2002.

Dimarogonas, A.D., "Vibration of Cracked Structures: A State of the Art Review", Engineering Fracture Mechanics, 55, 831-857, 1996.

Drysdale, R.G., Hamid, A.A. and Baker, L.R., Masonry Structures: Behavior and Design, Prentice-Hall, Englewood Cliffs, New Jersey, 1994.

Frisch-Fay, R., "Stability of Masonry Piers", International Journal of Solids and Structures, 11, 187-198, 1975.

Gürel, M.A. and Çılı, F., "Stability of Tilted Masonry Walls under Seismic Transverse Forces", Proceedings of the 2nd International Congress on Studies in Ancient Structures, İstanbul, 381-388, 2001.

Gürel, M.A. and Kısa, M., "Buckling of Slender Prismatic Columns with a Single Edge Crack under Concentric Vertical Loads", Turkish Journal of Engineering and Environmental Sciences, 29, 185-193, 2005.

Hendry, A.W., "Masonry Walls: Materials and Construction", Construction and Building Materials, 15, 323-330, 2001.

İnan, M., Strength of Materials, Ist. Tech. Univ. Foundation Istanbul, 1988, (in Turkish).

Kisa, M. and Brandon, J.A., "The Effects of Closure of Cracks on the Dynamics of a Cracked Cantilever Beam", Journal of Sound and Vibration, 238, 1-18, 2000.

Kisa, M., "Free Vibration Analysis of a Cantilever Composite Beam with Multiple Cracks", Composites Science and Technology, 64, 1391-1402, 2004.

La Mendola, L. and Papia, M., "Stability of Masonry Piers under Their Own Weight and Eccentric Load", Journal of Structural Engineering, ASCE, 119, 1678-1693, 1993.

La Mendola, L., Papia, M. and Zingone, G., "Stability of Masonry Walls Subjected to Seismic Transverse Forces", Journal of Structural Engineering, ASCE, 121, 1581-1587, 1995.

Lu, M., Schultz, A.E. and Stolarski, H.K., "Application of the Arc-Length Method for the Stability Analysis of Solid Unreinforced Masonry Walls under Lateral Loads", Engineering Structures, 27, 909-919, 2005.

Masia, M.J., Melchers, R.E. and Kleeman, P.W., "Probabilistic Crack Prediction for Masonry Structures on Expansive Soils", Journal of Structural Engineering, ASCE, 128, 1454-1461, 2002.

Nikpour, K., "Buckling of Cracked Composite Columns", International Journal of Solids and Structures, 26, 1371-1386, 1990.

Psycharis, I.N., Papastamatiou, D.Y. and Alexandris, A.P., "Parametric Investigation of the Stability of Classical Columns under Harmonic and Earthquake Excitations", Earthquake Engineering and Structural Dynamics, 29, 1093-1109, 2000.

Ranjbaran, A., "A Computer Model for the Analysis of Masonry Columns", Computers and Structures, 55, 543-551, 1995.

Romano, F., Ganduscio, S. and Zingone, G., "Cracked Nonlinear Masonry Stability under Vertical and Lateral Loads", Journal of Structural Engineering, ASCE, 119, 69-87, 1993.

Sucuoğlu, H. and Erberik, A., "Performance Evaluation of a Three-Storey Unreinforced Masonry Building During the 1992 Erzincan Earthquake", Earthquake Engineering and Structural Dynamics, 26, 319-336, 1997.

Tomaževič, M. and Klemenc, I., "Seismic Behavior of Confined Masonry Walls", Earthquake Engineering and Structural Dynamics, 26, 1059-1071, 1997.

Tomaževič, M., Earthquake-Resistant Design of Masonry Buildings, Imperial College Press. London, 1999.

Yokel, F.Y., "Stability and Load Capacity of Members with No Tensile Strength", Journal of the Structural Division, ASCE, 97, 1913-1926, 1971.